REPORT

Nanograded artificial nacre with efficient energy dissipation

Yu-Feng Meng,[1] Cheng-Xin Yu,[2,3] Li-Chuan Zhou,[4] Li-Mei Shang,[1] Bo Yang,[1] Qing-Yue Wang,[1] Xiang-Sen Meng,[1] Li-Bo Mao,[1,*] and Shu-Hong Yu[1,5,*]
*Correspondence: maolb@ustc.edu.cn (L.-B.M.); yush@sustech.edu.cn (S.-H.Y.)
Received: May 23, 2023; Accepted: August 27, 2023; Published Online: August 30, 2023; https://doi.org/10.1016/j.xinn.2023.100505
© 2023 The Authors. This is an open access article under the CC BY-NC-ND license (http://creativecommons.org/licenses/by-nc-nd/4.0/).

GRAPHICAL ABSTRACT

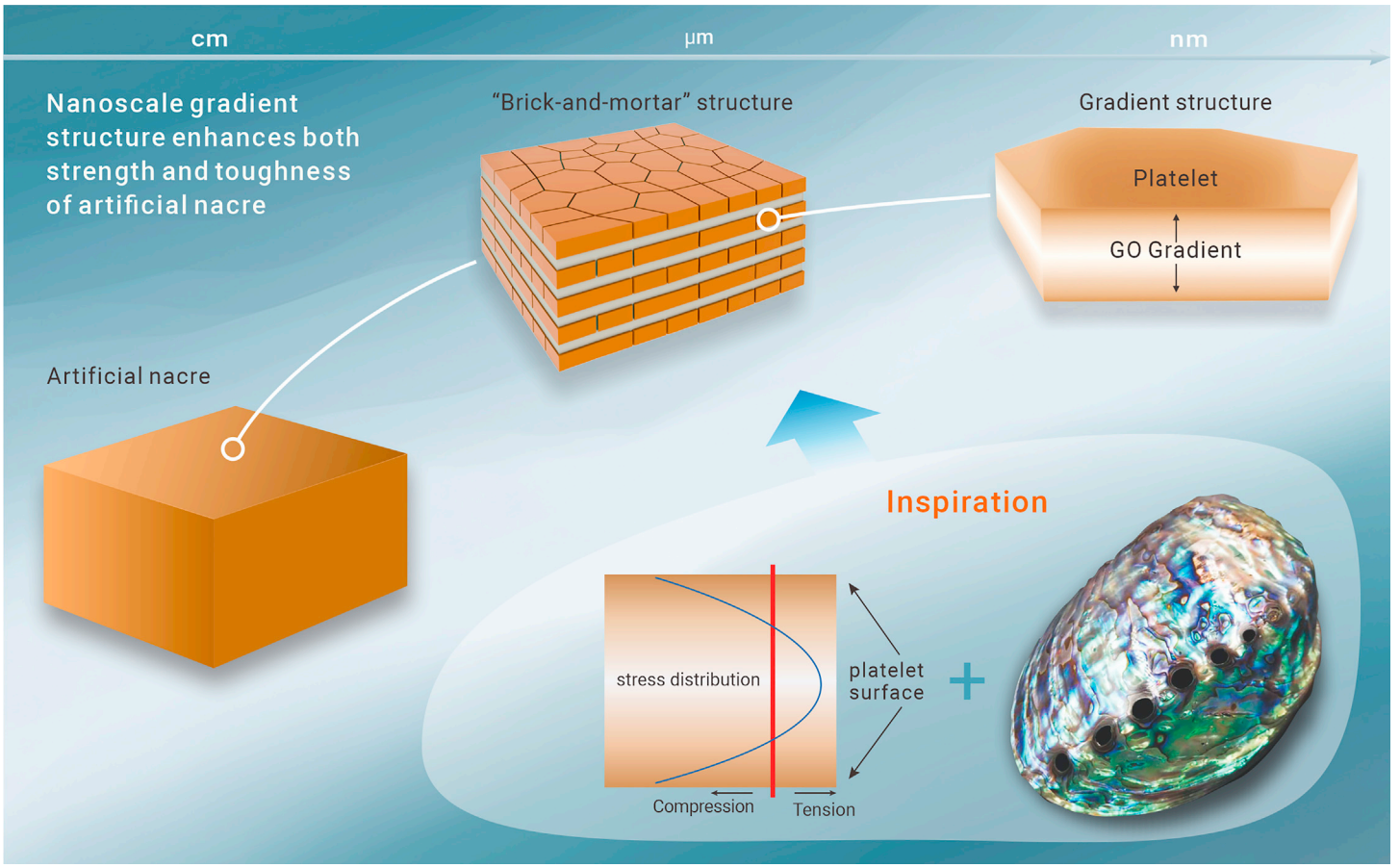

PUBLIC SUMMARY

- Nanoscale gradient is introduced into the mineral platelets of artificial nacre.
- The gradient structure is formed as the amorphous precursor crystallizes.
- Platelets enhanced by the gradient-induced prestress promote extrinsic toughening.
- Artificial nacre with nanogradient structure exhibits high energy dissipation.

REPORT

Nanograded artificial nacre with efficient energy dissipation

Yu-Feng Meng,[1] Cheng-Xin Yu,[2,3] Li-Chuan Zhou,[4] Li-Mei Shang,[1] Bo Yang,[1] Qing-Yue Wang,[1] Xiang-Sen Meng,[1] Li-Bo Mao,[1,*] and Shu-Hong Yu[1,5,*]

[1]Department of Chemistry, New Cornerstone Science Laboratory, Institute of Biomimetic Materials & Chemistry, Anhui Engineering Laboratory of Biomimetic Materials, Division of Nanomaterials & Chemistry, Hefei National Research Center for Physical Sciences at the Microscale, University of Science and Technology of China, Hefei 230026, China

[2]Key Laboratory of Materials Physics, Anhui Key Laboratory of Nanomaterials and Nanotechnology, CAS Center for Excellence in Nanoscience, Institute of Solid State Physics, Chinese Academy of Sciences, Hefei 230031, China

[3]Institute of Physical Science and Information Technology, Anhui University, Hefei 230601, China

[4]School of Mechanical Engineering, Hefei University of Technology, Hefei 230009, China

[5]Institute of Innovative Materials, Department of Materials Science and Engineering, Department of Chemistry, Southern University of Science and Technology, Shenzhen 518055, China

*Correspondence: maolb@ustc.edu.cn (L.-B.M.); yush@sustech.edu.cn (S.-H.Y.)

Received: May 23, 2023; Accepted: August 27, 2023; Published Online: August 30, 2023; https://doi.org/10.1016/j.xinn.2023.100505

© 2023 The Authors. This is an open access article under the CC BY-NC-ND license (http://creativecommons.org/licenses/by-nc-nd/4.0/).

Citation: Meng Y.-F., Yu C.-X., Zhou L.-C., et al., (2023). Nanograded artificial nacre with efficient energy dissipation. The Innovation **4(6)**, 100505.

The renowned mechanical performance of biological ceramics can be attributed to their hierarchical structures, wherein structural features at the nanoscale play a crucial role. However, nanoscale features, such as nanogradients, have rarely been incorporated in biomimetic ceramics because of the challenges in simultaneously controlling the material structure at multiple length scales. Here, we report the fabrication of artificial nacre with graphene oxide nanogradients in its aragonite platelets through a matrix-directed mineralization method. The gradients are formed via the spontaneous accumulation of graphene oxide nanosheets on the surface of the platelets during the mineralization process, which then induces a lateral residual stress field in the platelets. Nanoindentation tests and mercury intrusion porosimetry demonstrate that the material's energy dissipation is enhanced both intrinsically and extrinsically through the compressive stress near the platelet surface. The energy dissipation density reaches 0.159 ± 0.007 nJ/μm^3, and the toughness amplification is superior to that of the most advanced ceramics. Numerical simulations also agree with the finding that the stress field notably contributes to the overall energy dissipation. This work demonstrates that the energy dissipation of biomimetic ceramics can be further increased by integrating design principles spanning multiple scales. This strategy can be readily extended to the combinations of other structural models for the design and fabrication of structural ceramics with customized and optimized performance.

INTRODUCTION

Biological structural ceramics, despite being comprised of brittle minerals and weak macromolecules, exhibit extraordinary mechanical properties. For example, nacre, composed of aragonite platelets (>95 vol %) and biopolymers (<5 vol %), impressively reconciles high toughness and high strength via complex structural designs. These two properties are typically mutually exclusive in most artificial structural materials.[1,2] As a consequence, adopting biomimetic design principles presents an effective way to remedy the shortcomings of artificial materials, such as the inherent brittleness of ceramics.[3] The "brick-and-mortar" structure derived from nacre is one of the most accessed biomimetic models, by which the fracture toughness of artificial composites, such as ceramics, can be improved extrinsically.[4–8] In some cases, the apparent fracture toughness and strength of these nacre-mimetic structural ceramics even surpass those of natural nacre itself. Nevertheless, this achievement is primarily attributed to the higher toughness and strength of the raw materials employed in these artificial ceramics rather than to the effect of their structures.[7,9] In fact, the structure-associated fracture toughness amplification of these nacre-mimetic ceramics with respect to that of the raw materials is much less remarkable than that of natural nacre.[10,11]

By comparing biomimetic materials and their natural counterparts, the key factor that dramatically diverges the performance of the two can be revealed—while biomimetic materials can only roughly mimic the structure of biological ceramics, the true structures of biological ceramics are precisely controlled over several length scales to optimize their properties.[12–15] Taking the fine structure of nacre as an example, the organics not only reside between the aragonite platelets but also uniformly distribute within these platelets. The incorporated organics are considered to be the primary origin of the lattice distortion in aragonite crystals, which can eventually toughen nacre.[15] In addition, these platelets are not monolithic but are composed of tiny granules, a design that promotes zigzag crack propagation within the platelets. In contrast, in geological monolithic aragonite, cracks extend along cleavage planes and thus dissipate much less energy.[16]

In light of the precise structural tuning found in biological ceramics, recent efforts have demonstrated the mechanical performance of biomimetic materials can indeed be further reinforced.[8,17,18] However, the fine structure control of biomimetic materials remains largely unexplored. For example, despite some exceptions,[19] the platelet strength of many of the previously reported nacre-mimetic ceramics is insufficient to support platelet sliding during their failure,[4,7,20,21] which restricts the biomimetic toughening of these materials.[22] Therefore, a rational design to strengthen the platelets is pivotal to reach the higher fracture toughness of these ceramics. In this respect, many biological ceramics such as tooth enamel develop gradient structures that generate local prestress to optimize their mechanical and chemical performance. Besides, while it is challenging to precisely control such a complicated structure, evidence has also demonstrated that such gradients can be feasibly created by controlled mineralization.[12,23]

Inspired by the gradient structures of biological ceramics formed via biomineralization, we herein introduce composition gradients into the platelets of the artificial nacre via biomimetic mineralization. Experimental evidence suggests that the gradient induces compressive residual stress on the surface of the platelets, which is similar to that in tempered glass and thereby endows the platelets with increased strength as well as damage resistance. Therefore, the platelets can more effectively shield the crack propagation and sustain platelet sliding, by which the fracture toughness of the artificial nacre can be further improved. The present work provides a feasible strategy to realize the integration of multiscale structural designs, whereby biomimetic structural ceramics with superior performance can be fabricated.

RESULTS

Fabrication of artificial nacre with graphene oxide gradients

Artificial nacre with graphene oxide gradients (GAN) is fabricated by biomimetic mineralization on a laminated matrix containing graphene oxide nanosheets (Figure 1A). Specifically, a graphene oxide nanosheet suspension is added to a chitosan solution, which is followed by ultrasonication. The mixture is bidirectionally freeze casted, by which ice crystals grow in the form of well-aligned layers, and thus the solutes are spontaneously isolated from the solution and then compressed by the ice crystals into ordered layers. The graphene oxide-chitosan matrix with a lamellar architecture is obtained by lyophilization in a vacuum dryer and then transforms into a more stable graphene oxide-chitin matrix via acetylation. The matrix is immersed in a calcium bicarbonate solution in the presence of poly(acrylic acid) and Mg^{2+} and mineralized through a circulation system. The obtained mineralized matrix is dark colored due to the graphene oxide incorporation, while the control group, the artificial nacre with no graphene oxide (denoted as NGN), displays a white color. The GAN (Figure 1B, insert), as well as NGN, is obtained by hot pressing the mineralized matrix infiltrated with silk fibroin solution. Notably, while the graphene oxide content in the initial mixture can be tuned within a wide range, too much

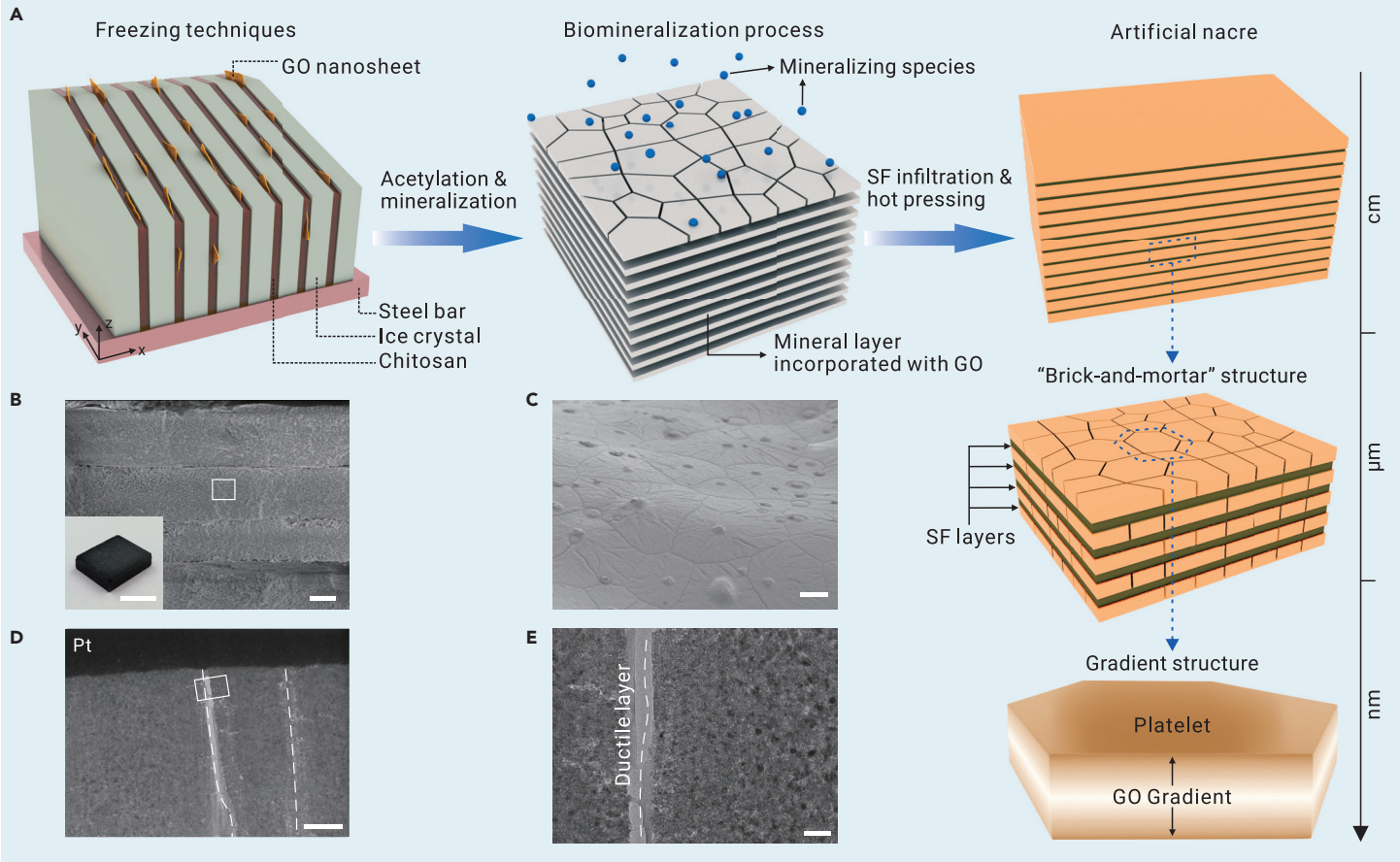

Figure 1. Multiscale design principles of GAN (A) Schematic illustration of the fabrication process, and the hierarchical structure of the GAN. (B) Fractured surface of the GAN showing a typical laminated structure. Inset: the GAN bulk. (C) Aragonite platelets of the GAN. (D) TEM image of adjacent aragonite platelets separated by silk fibroin (SF) layers. The white dashed lines indicate the ductile SF layers. (E) Magnified TEM image of the nanograins in (D). Scale bars are 1 μm (inset: 1 cm), 50 μm, 1 μm, and 400 nm for (B)–(E). GO, graphene oxide.

graphene oxide can retard the mineralization of the matrix, leading to structural defects, which cause unfavorable changes to the properties of the GAN (Figures S3 and S4). To avoid this, the graphene oxide content in the unmineralized matrix before acetylation is fixed at 20 wt % in this study (supplemental discussion 1).

Structure and composition analyses

The GAN shows a nacre-mimetic hierarchical structure. The bulk consists of alternating calcium carbonate mineral layers and ductile silk fibroin layers with long-range order (Figure 1B). The mineral layers are composed of platelets with distinct borders instead of extremely large continuous layers (Figure 1C). Nevertheless, the graphene oxide-chitin matrix has been assimilated into the mineral platelets; fragments of the matrix can be found in the platelets (Figure S5). In addition, owing to the biomimetic mineralization and hot-pressing treatment, dovetails of the platelets and waviness structure of the platelet stacking, both of which are typical features of natural nacre, also exist in the GAN (Figure S6). At an even smaller scale, the platelets are not monolithic but formed by closely packed nanograins with diameters ranging from 10 to 100 nm (Figures 1D, 1E, and S7). The NGN exhibits the same nacre-mimetic structure as the GAN does, indicating that the addition of a moderate amount of graphene oxide nanosheets does not noticeably change the microstructure of the materials (Figure S8). The GAN and the NGN contain similar fractions of calcium carbonate (Figure S2). Nevertheless, compared with the single aragonite phase of the mineral in the NGN, a weak diffraction peak at approximately 13.1° in the synchrotron high-resolution powder X-ray diffraction spectrum discloses the presence of a small amount of calcite in the GAN (Figure S9). Rietveld structure refinement shows that the crystalline minerals comprise 8.9 wt % calcite and 91.1 wt % aragonite.[24] This suggests that graphene oxide can interact with calcium carbonate and thus affect its crystallization. The peaks related to aragonite also shift and broaden after the incorporation of graphene oxide, which reveals the aragonite lattice distortion induced by the graphene oxide (Figure S10). This direct evidence indicates the interaction between graphene oxide and the minerals,[25] which agrees well with the previous analysis.

While the distribution of graphene oxide nanosheets cannot be identified solely by the observations on the hierarchical structure of the GAN, this can be revealed by correlative Raman imaging and scanning electron microscopy, which enables the acquisition of both the chemical information and the morphological image of a selected area with nanoscale precision. The aragonite and the graphene oxide are particularly distinguishable by Raman spectroscopy: the former has a strong $\nu 1$ peak at about 1,085 cm^{-1}, which is associated with the symmetric stretching of C–O bonds in CO_3^{2-} units,[26] while the latter shows characteristic D and G Raman bands between 1,300 and 1,650 cm^{-1} (Figure 2A). By collecting the Raman spectra of all the pixels in the selected area on a polished cross-sectional surface of the sample (Figure 2B), the peak areas of the aragonite at 1,085 cm^{-1} and the G band of the graphene oxide of each pixel are calculated, respectively. Consequently, the relative distribution of the aragonite and graphene oxide can then be plotted based on the area data of the pixels (Figure 2C). The results illustrate that, while the platelet primarily consists of aragonite, the graphene oxide nanosheets accumulate near the interlamellar surface of the platelet and become less concentrated at the center (Figure 2D). The formation of such a graphene oxide gradient along the thickness direction of the mineral platelets can be attributed to the mineralization process of calcium carbonate. In the mineralizing solution, amorphous calcium carbonate nanoparticles that are probably stabilized by the additives form from the initial solution (Figures 2E, inset, and S11) and can be verified by the selected-area electron diffraction of these nanoparticles (Figure 2E). These precursory nanoparticles precipitate on the graphene oxide-chitin matrix. As these amorphous nanoparticles gradually crystallize into aragonite and then ripen, graphene oxide nanosheets, which exist in the platelets as impurities, can be expelled to the platelet surface.[12,25,27]

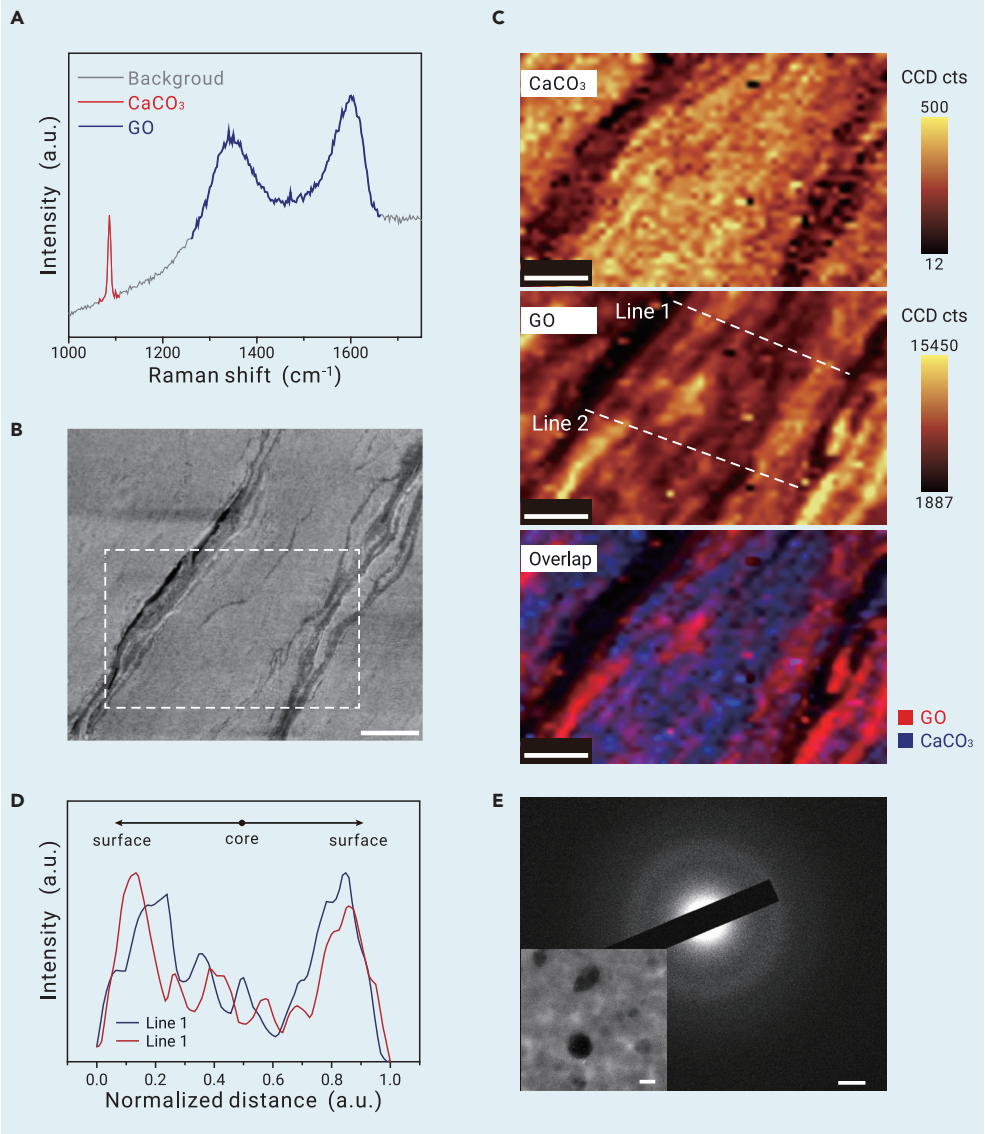

Figure 2. Graphene oxide gradient structure in mineral layer (A) Typical Raman spectra of the GAN. GO, graphene oxide. (B) Scanning electron microscopy (SEM) image of the fractured surface of the GAN. (C) Correlative Raman-SEM image of the area in the white dashed line in (B), showing Raman mapping of the $CaCO_3$ (1,085 cm^{-1}), graphene oxide (1,650 cm^{-1}), and the overlap of the two images. (D) Line scans of the graphene oxide G band peak area extracted from (C), which reveal a graphene oxide gradient along the platelet thickness direction. (E) Selected-area electron diffraction pattern of the dried mineralizing solution sample. Inset: the corresponding TEM image. Scale bars are 5 μm, 5 μm, 2 1/nm, and 100 nm for (B), (C), (E), and the inset of (E), respectively.

Microscopic mechanical performance

The GAN exhibits distinct behavior in the nanoindentation tests compared with geological aragonite and calcite. There are no cracks around the indents on the surface of the former, and the crush of the indenter tip causes severe cracks and fractures around the indents in the latter (Figure S12). To gain further insights into the damage resistance of the GAN at the platelet level, the subsurface region under the indent is observed by a cross-sectional transmission electron microscope, showing a permanent triangular crater created by the indenter tip (Figure 3A–I). The main crack is highly localized, and no large lateral crack can be found around the indent, while the indent in geological calcium carbonate reveals notable main crack propagation and lateral crack generation.[28] There are several energy dissipation mechanisms in the GAN (Figure 3A–II). The nanogranular structure, which is similar to that in natural nacre, allows nanograin plastic deformation due to rotation and deformation that results in a pile-up zone around the indent.[29] The nanograins in the pile-up regions can even fuse and recrystallize into larger grains, which can be verified by the selected-area electron diffraction of this region (Figure 3A–III). In addition, the formation of crack bridging and nanocracks in the vicinity of the indent can further dissipate energy.

Although both samples display the same energy dissipation mechanisms, their nanoindentation behavior is quite different. The nanoindentation hardness of the GAN is 50% higher than that of the NGN, while the modulus increases slightly (Figure S13A). In the displacement-control regime, while the load on the NGN platelet is only about 3.8 ± 0.3 mN at an indentation depth of 1 μm, the load on the GAN platelet is 6.9 ± 0.2 mN at the same depth (Figure S13B). However, the deformed region around the indent on the GAN is reversely smaller than that of the NGN. Larger fusion regions and many more nanocracks can be found around the indent on the latter (Figure S14). These indicate that, to resist the crush of the indenter tip, it requires activating less inelastic deformation in the GAN than in the NGN. We further calculate the energy dissipation density by the ratio of the encircled area under the load-displacement curve to the corresponding volume of the plastic region. The energy dissipation density of the GAN reaches 0.159 ± 0.007 nJ/μm^3, which doubles that of the NGN with a value of 0.072 ± 0.007 nJ/μm^3 (Figure 3B).

As the structure and the composition of both the GAN and the NGN are similar, the difference between their properties can be attributed to the incorporation of graphene oxide. It has been reported that reduced graphene oxide can toughen ceramics at the price of lowering the strength and hardness[30] and thus is not considered a good strengthening agent for brittle ceramics. Nevertheless, the inhomogeneous distribution of graphene oxide can trigger another mechanism to harden and strengthen the platelet. The effect of such inhomogeneity on calcium carbonate is unraveled by preparing a wet double-layered calcium carbonate/graphene oxide composite film, where the layers contain different amounts of graphene oxide.[24] After drying, the film bends toward the side with less graphene oxide, indicating that the incorporation of graphene oxide can suppress the lateral shrinkage of the wet calcium carbonate during drying (Figure S15). Therefore, as the geometry is constrained, the graphene oxide gradient in the platelet of the GAN leads to the generation of lateral compressive residual stress near the surface, as well as the compensating tensile residual stress in the core with less graphene oxide (Figure S16A). In addition, further direct evidence of the residual stress is provided by nanoindentation tests on the lateral surface of the platelet. The hardness profile along the thickness direction of the platelet shows that the hardness of the surface is smaller than that of the core, which can be attributed to the compressive stress near the surface and the tensile stress near the core (Figures 3C, 3D, and S17).[31,32] The compressive stress can help resist the crack initiation at the defect sites near the surface of the platelet induced by the external stress. This also explains the different behaviors of the GAN and the NGN in the nanoindentation tests (Figures 3A, S13, and S14). A similar mechanism has been studied and used for producing tempered glass, which has superior strength and resistance to impact and scratch.[33–35] We perform finite element analysis on a single mineral platelet with/without

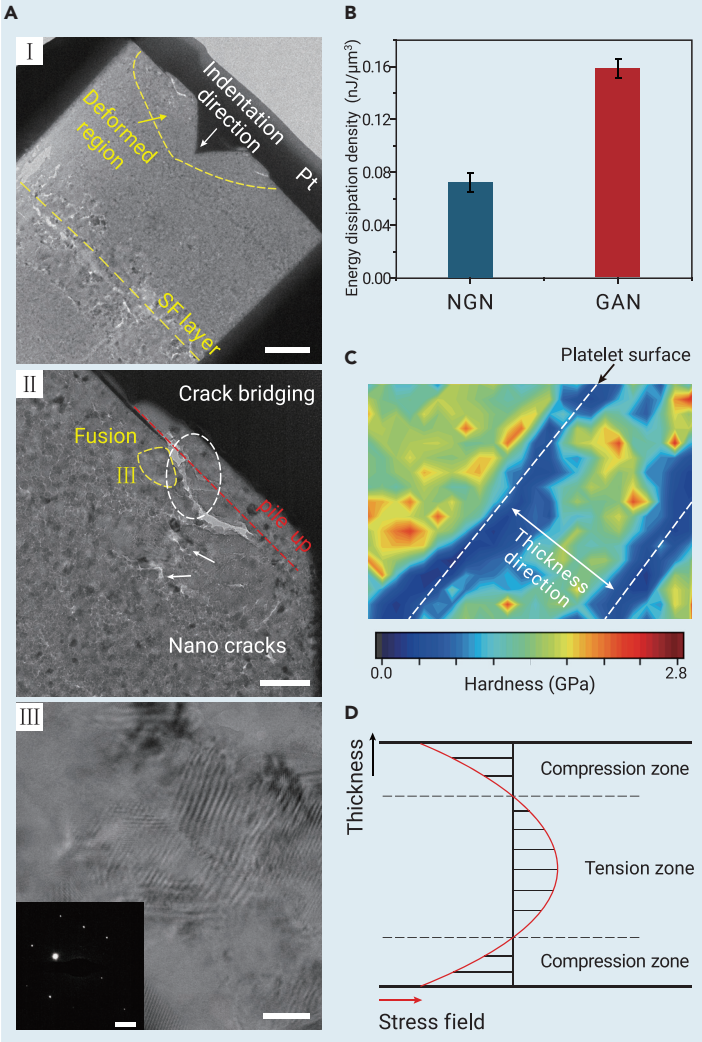

Figure 3. Microscopic mechanical performance (A) TEM image of the permanently deformed indent region in the GAN, where Pt represents the protective platinum layer (I). Enlarged view of the plastic region showing the fusion, nanocracks, and crack bridging (II). High-resolution TEM image of the fusion region denoted by a yellow line in (I) and (II) and the corresponding selected-area electron diffraction pattern (III). Scale bars are 1 μm, 200 nm, 20 nm, and 5 1/nm for (I), (II), (III), and the inset of (III), respectively. (B) Energy dissipation density is determined by the indentation tests. Each sample was tested at least 3 times. (C) Large-area nanoindentation hardness mapping of the cross-section of the GAN (red dashed line in Figure S17). (D) Schematic diagram of the residual stress field in the platelet of the GAN.

gradient-induced residual stress field. The model is based on tensile stress rather than the crush of the indenter, as a relationship has been established between the tensile strength and the hardness.[36] The results illustrate that, with higher field strength, the platelet shows higher tensile strength (Figure S16B).

Macroscopic mechanical performance

The incorporation of the graphene oxide gradients into the platelets notably affects the macroscopic mechanical performance of the artificial nacre, although the GAN and the NGN share a similar nacre-mimetic structure (Figure 4). The flexural strength increases from 66.6 ± 2.3 MPa of the NGN to 94.2 ± 3.5 MPa of the GAN, whereas the deformability is also improved (Figure 4A). The strengthening of the artificial nacre does not cause a decrease in the toughness, which is commonly seen in structural materials.[1] We evaluate the toughness of both samples via single-edge-notched beam tests. The rising crack resistance curves indicate the contribution of the extrinsic toughening mechanism to the overall toughness. As the crack grows, the fracture toughness of the GAN reaches 2.95 ± 0.11 MPa $m^{1/2}$ at the end of the stable crack growth stage, which is estimated to be 33% higher than that of the NGN (Figure 4B).

To analyze the origin of the improved fracture toughness, we divide the *J*-integral-based fracture toughness K_{Jc} into the intrinsic part K_{Ic}, which acts ahead of the crack tip, and the extrinsic part $K_{Jc} - K_{Ic}$, which comes into effect in the wake of the crack. Both parts of the GAN are found to be higher than those of the NGN (Figure 4C). For the intrinsic part, as shown in the nanoindentation analyses, the compressive residual stress field near the surface of the platelet in the GAN provides additional resistance to the lateral tensile force and makes the platelet less sensitive to surface defects. Given that the cracks often initiate at the platelet surface, despite the tensile residual stress at the core of the platelet, such a design ensures that the platelets can better arrest or deflect cracks. For the extrinsic part, because the compressive residual stress near the platelet surface can strengthen the platelet against tensile stress,[35] the platelet can more effectively be pulled out and slide during the fracture. This can be evidenced by the much larger specific pits/gaps volume on the fracture surface of the GAN measured by mercury intrusion porosimetry (Figure 4D).[18] Thereby, more energy can be dissipated extrinsically in the GAN.[22,37] This is in line with the discrete element modeling result that illustrates that platelets with strength gradients enable more platelet sliding and extrinsic mechanisms (Figures 4E–4G). Besides the contribution of the residual stress field generated by the gradients, it has been reported that the incorporation of the graphene oxide nanosheets can also reduce the brittleness of the materials.[38] Yet the role of this mechanism should be limited because no obvious pull out of graphene oxide on the fractured surface of the platelet in the GAN has been observed. Taken together, the residual stress gradients induced by the graphene oxide gradients in the platelets can improve the fracture toughness both intrinsically and extrinsically. Interestingly, the simulations of the fracture of the GAN samples with different residual stress gradients suggest that the energy dissipation capability of the GAN can be further enhanced by amplifying the gradients, although the balance between the compressive stress and tensile stress remains untouched (Figures 4H and 4I).

DISCUSSION

In summary, we report the fabrication of nanograded artificial nacre via a biomimetic mineralization method. Driven by the crystallization of the mineral precursors, the nanosheets aggregate near the surface of the platelets in the artificial nacre, and thus graphene oxide gradients are established in mineral platelets. Such gradients induce a compressive stress field near the surface by which the platelet hardness and strength and the resistance to crack initiation near the platelet surface are improved. With the merit of the nacre-mimetic structure at the microscale, the platelets in the artificial nacre with gradients can better shield the cracks and slide in the crack wake and thereby exhibit both higher intrinsic and extrinsic fracture toughness compared with that of artificial nacre without gradient. The toughness amplification can reach 14.7 ± 0.55, which outperforms the most advanced ceramics (Figure S18).[18]

Our work exemplifies that the integration of design principles at different levels, regardless of whether they are bioinspired or not, can substantially promote the mechanical performance of structural ceramics. Nevertheless, the combinations of many other design principles in different material systems are yet to be assessed. Future efforts should focus on developing fabrication techniques to achieve the integration of multiple structural designs in a controllable way and analyzing the outcome of these combinations via both experiments and simulations. We anticipate that such a strategy can eventually lead to the fabrication of unprecedented structural materials with exceeding and adjustable performance.

MATERIAL AND METHODS

See the supplemental information for details.

DATA AND CODE AVAILABILITY

All data needed to evaluate the conclusions in the paper are present in the paper and/or the supplemental information.

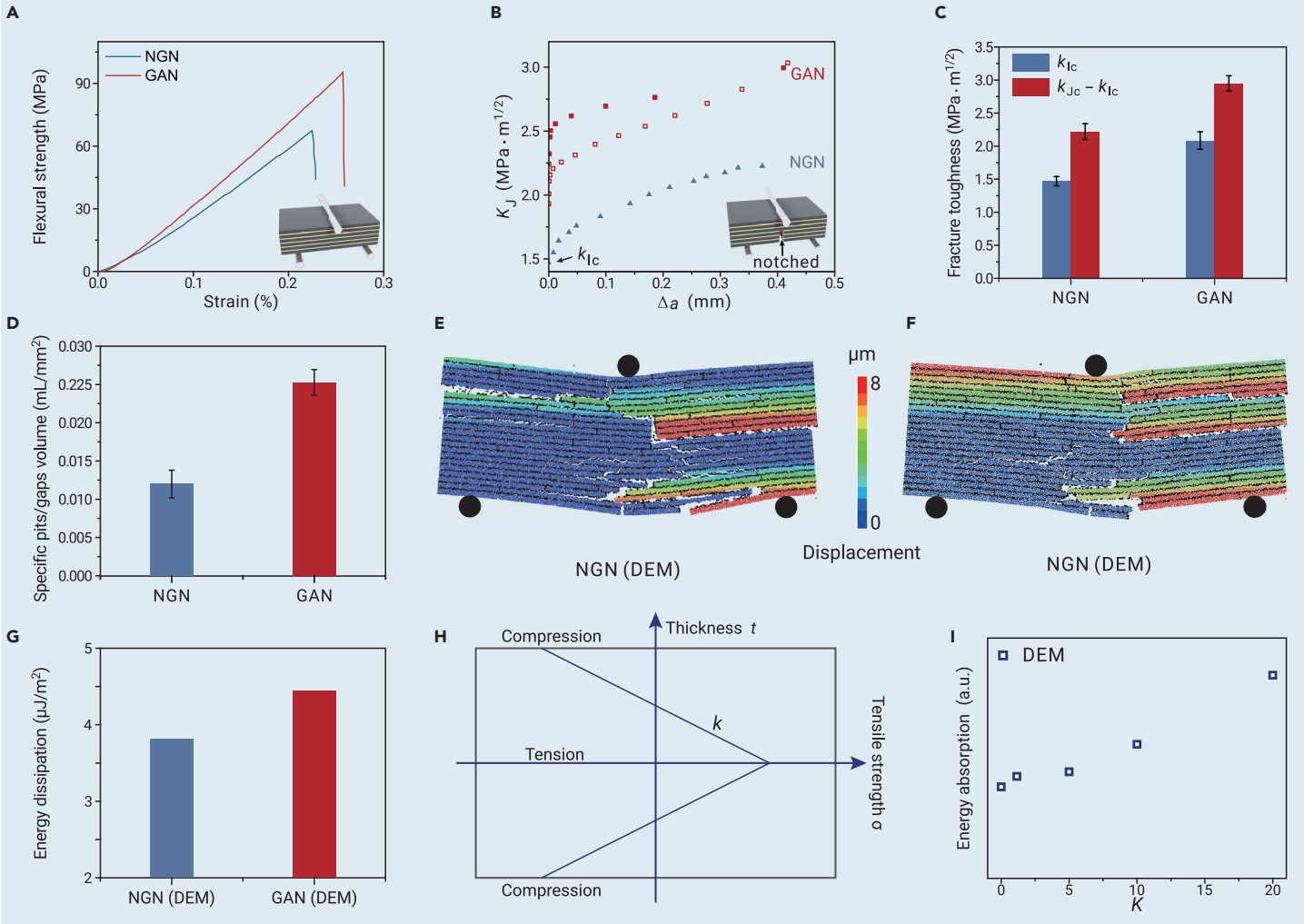

Figure 4. Macroscopic mechanical performance (A) Flexural stress-strain curves of the NGN and the GAN. Each sample was tested at least three times. (B) Crack resistance curves of the NGN and the GAN. Each sample was tested at least three times. (C) Histogram of the intrinsic and the extrinsic toughness of the NGN and the GAN. (D) Cumulative intrusion of mercury of the fractured surface of the NGN and the GAN. Each sample was tested at least 3 times. (E and F) Discrete element modeling analysis of the behaviors of the NGN (E) and the GAN (F) in three-point bending tests. The platelet sliding can be visualized by the increasing displacement (from blue to red). (G) Energy dissipation of the NGN and the GAN obtained from the simulation. (H) Illustration of the platelet tensile strength distribution along the platelet thickness direction used for discrete element modeling simulation, which is induced by the residual stress field. The line slope k (σ/t) is associated with the graphene oxide gradients. (I) Overall energy dissipation increases as the slope k increases, which is calculated based on the discrete element modeling in a similar way to those in (E) and (F). DEM, discrete element method.

REFERENCES

1. Ritchie, R.O. (2011). The conflicts between strength and toughness. Nat. Mater. ***10***, 817–822.
2. Meyers, M.A., McKittrick, J., and Chen, P.-Y. (2013). Structural biological materials: Critical mechanics-materials connections. Science ***339***, 773–779.
3. Nepal, D., Kang, S., Adstedt, K.M., et al. (2023). Hierarchically structured bioinspired nanocomposites. Nat. Mater. ***22***, 18–35.
4. Mao, L.B., Gao, H.L., Yao, H.B., et al. (2016). Synthetic nacre by predesigned matrix-directed mineralization. Science ***354***, 107–110.
5. Gao, H.L., Chen, S.M., Mao, L.B., et al. (2017). Mass production of bulk artificial nacre with excellent mechanical properties. Nat. Commun. ***8***, 287.
6. Das, P., Malho, J.-M., Rahimi, K., et al. (2015). Nacre-mimetics with synthetic nanoclays up to ultrahigh aspect ratios. Nat. Commun. ***6***, 5967.
7. Bouville, F., Maire, E., Meille, S., et al. (2014). Strong, tough and stiff bioinspired ceramics from brittle constituents. Nat. Mater. ***13***, 508–514.
8. Grossman, M., Bouville, F., Masania, K., et al. (2018). Quantifying the role of mineral bridges on the fracture resistance of nacre-like composites. Proc. Natl. Acad. Sci. USA ***115***, 12698–12703.
9. Munch, E., Launey, M.E., Alsem, D.H., et al. (2008). Tough, bio-inspired hybrid materials. Science ***322***, 1516–1520.
10. Pro, J.W., and Barthelat, F. (2019). The fracture mechanics of biological and bioinspired materials. MRS Bull. ***44***, 46–52.
11. Wegst, U.G.K., Bai, H., Saiz, E., et al. (2015). Bioinspired structural materials. Nat. Mater. ***14***, 23–36.
12. DeRocher, K.A., Smeets, P.J.M., Goodge, B.H., et al. (2020). Chemical gradients in human enamel crystallites. Nature ***583***, 66–71.
13. Bianco-Stein, N., Polishchuk, I., Lang, A., et al. (2022). High-Mg calcite nanoparticles within a low-Mg calcite matrix: A widespread phenomenon in biomineralization. Proc. Natl. Acad. Sci. USA ***119***, e2120177119.
14. Shin, Y.A., Yin, S., Li, X., et al. (2016). Nanotwin-governed toughening mechanism in hierarchically structured biological materials. Nat. Commun. ***7***, 10772.
15. Gim, J., Schnitzer, N., Otter, L.M., et al. (2019). Nanoscale deformation mechanics reveal resilience in nacre of Pinna nobilis shell. Nat. Commun. ***10***, 4822.
16. Huang, Z., and Li, X. (2013). Origin of flaw-tolerance in nacre. Sci. Rep. ***3***, 1693.
17. Zhao, H., Liu, S., Wei, Y., et al. (2022). Multiscale engineered artificial tooth enamel. Science ***375***, 551–556.
18. Meng, Y.F., Zhu, Y.B., Zhou, L.C., et al. (2022). Artificial Nacre with High Toughness Amplification Factor: Residual Stress-Engineering Sparks Enhanced Extrinsic Toughening Mechanisms. Adv. Mater. ***34***, e2108267.
19. Yin, Z., Hannard, F., and Barthelat, F. (2019). Impact-resistant nacre-like transparent materials. Science ***364***, 1260–1263.
20. Picot, O.T., Rocha, V.G., Ferraro, C., et al. (2017). Using graphene networks to build bioinspired self-monitoring ceramics. Nat. Commun. ***8***, 14425.
21. Wat, A., Lee, J.I., Ryu, C.W., et al. (2019). Bioinspired nacre-like alumina with a bulk-metallic glass-forming alloy as a compliant phase. Nat. Commun. ***10***, 961.
22. Barthelat, F. (2014). Designing nacre-like materials for simultaneous stiffness, strength and toughness: Optimum materials, composition, microstructure and size. J. Mech. Phys. Solid. ***73***, 22–37.
23. Amini, S., Tadayon, M., Loke, J.J., et al. (2019). A diecast mineralization process forms the tough mantis shrimp dactyl club. Proc. Natl. Acad. Sci. USA ***116***, 8685–8692.
24. Details Are Available in Supplementary Materials and Methods.
25. Giosia, M.D., Polishchuk, I., Weber, E., et al. (2016). Bioinspired Nanocomposites: Ordered 2D Materials Within a 3D Lattice. Adv. Funct. Mater. ***26***, 5569–5575.
26. DeCarlo, T.M. (2018). Characterizing coral skeleton mineralogy with Raman spectroscopy. Nat. Commun. ***9***, 5325.

27. Politi, Y., and Weaver, J.C. (2015). Biomineralization. Built for tough conditions. Science ***347***, 712–713.
28. Li, L., and Ortiz, C. (2014). Pervasive nanoscale deformation twinning as a catalyst for efficient energy dissipation in a bioceramic armour. Nat. Mater. ***13***, 501–507.
29. Li, X. (2007). Nanoscale structural and mechanical characterization of natural nanocomposites: Seashells. Jom ***59***, 71–74.
30. Li, Q., Zhang, Y., Gong, H., et al. (2016). Enhanced Fracture Toughness of Pressureless-sintered SiC Ceramics by Addition of Graphene. J. Mater. Sci. Technol. ***32***, 633–638.
31. Jang, J.I. (2009). Estimation of residual stress by instrumented indentation: A review. J. Ceram. Process. Res. ***10***, 391–400.
32. Chang, L.-C., Zheng, Y.-Z., and Chen, Y.-I. (2018). Mechanical Properties of Zr–Si–N Films Fabricated through HiPIMS/RFMS Co-Sputtering. Coatings ***8***, 263.
33. Humood, M., Beheshti, A., and Polycarpou, A.A. (2017). Surface reliability of annealed and tempered solar protective glasses: Indentation and scratch behavior. Sol. Energy ***142***, 13–25.
34. Tandon, R., and Cook, R.E. (1993). Indentation Crack Initiation and Propagation in Tempered Glass. J. Am. Ceram. Soc. ***76***, 885–889.
35. Zhang, Y., Wang, W.H., and Greer, A.L. (2006). Making metallic glasses plastic by control of residual stress. Nat. Mater. ***5***, 857–860.
36. Amini, S., and Miserez, A. (2013). Wear and abrasion resistance selection maps of biological materials. Acta Biomater. ***9***, 7895–7907.
37. Shao, Y., Zhao, H.-P., Feng, X.-Q., et al. (2012). Discontinuous crack-bridging model for fracture toughness analysis of nacre. J. Mech. Phys. Solid. ***60***, 1400–1419.
38. Sun, C., Huang, Y., Qiang, S., et al. (2020). Embedding two-dimensional graphene array in ceramic matrix. Sci. Adv. ***6***, eabb1338.

ACKNOWLEDGMENTS

The authors thank Ming-Hui Fan and Zhi Zhao (USTC) for help with Raman testing, Hui-Juan Wang and Jie Tian (USTC) for help with transmission electron microscopy (TEM) testing, Tao Ma for assisting in synthesizing GO, and Bing Qin for helping polish samples. This work was supported by the Strategic Priority Research Program of the Chinese Academy of Sciences (XDB 0470000), the National Key Research and Development Program of China (2018YFE0202201 and 2021YFA0715700), and the National Natural Science Foundation of China (22305240 and 22293044). Y.-F.M. acknowledges the funding supported by the Students' Innovation and Entrepreneurship Foundation of USTC (XY2022S02) and the Double First-Class University Construction Fund from USTC (YD2060002037). This work has been supported by the New Cornerstone Science Foundation. This work was partially carried out at the USTC Center for Micro- and Nanoscale Research and Fabrication. This research used Beamline BL14B and BL15U of the Shanghai Synchrotron Radiation Facility (SSRF).

AUTHOR CONTRIBUTIONS

S.-H.Y. and L.-B.M. conceived the idea and designed the experiments. Y.-F.M., C.-X.Y., L.-M.S., B.Y., Q.-Y.W., and X.-S.M. carried out the experiments and characterizations. L.-C.Z. analyzed the data and provided theory support. Y.-F.M., L.-B.M., and S.-H.Y. wrote the manuscript.

DECLARATION OF INTERESTS

The authors declare no competing interests.

SUPPLEMENTAL INFORMATION

It can be found online at https://doi.org/10.1016/j.xinn.2023.100505.

LEAD CONTACT WEBSITE

http://staff.ustc.edu.cn/~yulab/